Applied Catalysis B: Environmental 164 (2015) 462–474

Contents lists available at ScienceDirect

Applied Catalysis B: Environmental

journal homepage: www.elsevier.com/locate/apcatb

Photocatalytic removal of atrazine using N-doped TiO_2 supported on phosphors

Olga Sacco[a,b], Vincenzo Vaiano[b,*], Changseok Han[a], Diana Sannino[b], Dionysios D. Dionysiou[a,c,**]

[a] Environmental Engineering and Science Program, Department of Biomedical, Chemical and Environmental Engineering, University of Cincinnati, Cincinnati, OH 45221-0012, USA
[b] University of Salerno, Department of Industrial Engineering, Via Giovanni Paolo II 132, 84084 Fisciano (SA), Italy
[c] Nireas-International Water Research Centre, University of Cyprus, 20537 Nicosia, Cyprus

ARTICLE INFO

Article history:
Received 9 July 2014
Received in revised form
22 September 2014
Accepted 24 September 2014
Available online 2 October 2014

Keywords:
$N\text{-}TiO_2$
ZnS-based phosphors
Photocatalysis
Atrazine pesticide.

ABSTRACT

Visible light-active N-doped TiO_2 ($N\text{-}TiO_2$) was successfully immobilized on ZnS-based phosphors microparticles (ZSP) by a modified sol–gel method. Core-shell catalysts were prepared to serve as "photoactive support", able to harvest the external irradiation and to emit a luminescence with wavelength suitable for activation of N-doped TiO_2. The nominal loading of $N\text{-}TiO_2$ on ZSP was in the range of 15–50 wt% and the effect of the progressive increase in $N\text{-}TiO_2$ loading on the coverage of phosphors particles was evaluated. The preparation method did not induce alterations of the initial ZSP crystallographic structure and allowed to obtain $N\text{-}TiO_2$ dispersion on ZSP surface. By varying the $N\text{-}TiO_2$ loadings on the surface of ZSP, its morphology gradually evolved from pseudo-spherical shape, until 30 wt% $N\text{-}TiO_2$ loading, to elongated shape for an $N\text{-}TiO_2$ content of 50 wt%. The photocatalytic activity of $N\text{-}TiO_2$/ZSP was evaluated for the removal of atrazine under UVA light irradiation. Enhanced performance compared to either pure $N\text{-}TiO_2$ nanoparticles or bare ZSP was observed. The photocatalyst $N\text{-}TiO_2$/ZSP at 30 wt% of $N\text{-}TiO_2$ loading (30$N\text{-}TiO_2$/ZSP) demonstrated the highest photocatalytic activity. Photocatalytic performances were strongly dependent on the concentration of catalyst and the initial pH of solution. The optimal catalyst concentration was 0.5 g L^{-1} and the optimal initial pH was 5.8. A study of the reaction intermediates during the photocatalytic removal of atrazine was carried out, evidencing that the sequence of intermediates for 30$N\text{-}TiO_2$/ZSP and for the phosphors ZSP alone included dealkylation reactions and alkyl chain oxidation.

1. Introduction

Persistent organic pollutants (POPs) have been identified as an increasing problem in drinking water supplies [1]. Such substances can enter the water supply from various sources and are not effectively removed by conventional water treatment processes [2]. Pesticides have been classified as POPs due to their resistance to natural removal processes and hence ability to remain in the environment for long periods of time. Atrazine (2-chloro-4-ethyl-amino-6-isopropylamino-1,3,5-triazine) is one of the most common pesticides found in groundwater sources and drinking water supplies. It is possible to remove atrazine in water by a photocatalytic process involving TiO_2 [3–6] or other types of photocatalysts such as ZnO and Fe_2O_3 [7].

However, the practical applications of the photocatalytic process are greatly hindered by the insufficient quantum efficiency of photocatalytic reactions which result from the relatively high recombination rate of photogenerated electron (e^-)–hole (h^+) pairs. Therefore, the major challenge in this area is to improve the photoactivity by minimizing the charge recombination. For this purpose, a variety of strategies have been utilized to promote the photoinduced charge carrier separation [8]. This can be achieved by coupling TiO_2 with another semiconductor [9]. Once both semiconductors are excited by light, e^- accumulate at the low-lying conduction band of one semiconductor, while h^+ accumulate at the valence band of the other material. These processes of charge separation are very fast and the efficiency of reduction or oxidation of the adsorbed organics remarkably increases [8]. TiO_2/CdS [10],

* Corresponding author. Tel.: +39 089 964006; fax: +39 089 964057.
** Corresponding author. Tel.: +1 513 556 0724; fax: +1 513 556 2599.
E-mail addresses: vvaiano@unisa.it (V. Vaiano), dionysios.d.dionysiou@uc.edu (D.D. Dionysiou).

http://dx.doi.org/10.1016/j.apcatb.2014.09.062
0926-3373/

TiO_2/CdSe [11], TiO_2/PbS [12], TiO_2/PbSe [13] or TiO_2/Cu-doped ZnS [8] heterojunctions have been widely studied in recent years in the photocatalytic removal of contaminants. In the case of TiO_2/Cu-doped ZnS, the enhanced photocatalytic activity is attributed to the ability of Cu-doped ZnS to generate hydroxyl radicals once associated to TiO_2 [8].

In addition, the photocatalytic reaction rate can be enhanced by doping TiO_2 with some metal and non-metal elements [14–21], increasing the specific surface area [22] and improving photocatalytic reactor design [23,24]. The key parameter is the photon distribution inside the reactor that should be uniform to effectively irradiate the photocatalysts [23,25,26]. Sannino et al. [25,27] reported a significant improvement of VO_x/TiO_2 photocatalytic activity in the selective partial oxidation of ethanol to acetaldehyde by the simultaneous irradiation with light emitting phosphorescent particles (phosphors) and UVA-LEDs as external light source. In this case, the photoreactivity was enhanced because the suitable phosphors introduced into the system were able to transform 365 nm radiation into 440 nm emission, able as well to photoexcite the fraction of photocatalyst in the core reactor volume, otherwise screened by the photocatalyst itself [27]. The results underlined as the higher capture of the photocatalyst, due to the additional light harvesting of support, gives enhanced activity in the selective oxidation of ethanol to acetaldehyde [27].

Among all photoluminescent semiconductors, ZnS-based phosphors (ZSP), associated with TiO_2, could increase the photocatalytic activities for decomposing contaminants because the recombination of charge carriers was retarded and the photons transfer inside the photoreactor could be enhanced [27,28].

To fruitfully capture the visible light emitted by ZSP, it is necessary to modify the TiO_2 photocatalyst to make it active in the presence of visible light.

Recently, intensive efforts have been directed to improve the photocatalytic behavior of TiO_2 under visible light, using transition metal (Fe, Co, Ag and Ni) [29,30] and non-metal (C, N, F and S) [18,20,21] dopants. Transition metal-doped TiO_2 has certain disadvantages such as low thermal stability and increased recombination of charge carriers leading to a low quantum yield. Synthesis of non-metal-doped TiO_2 has been suggested in order to avoid these drawbacks [31]. Among all, N-doped TiO_2 seems to be the most promising visible light absorbing photocatalyst [32–34]. It has shown that visible light can selectively promote the electrons from the N 2p states to the conduction band [32–34].

In this work, N-doped TiO_2 photocatalyst was immobilized on the surface of ZPS (N-TiO_2/ZSP) to synthesize core-shell photocatalysts. The N-TiO_2/ZSP photocatalysts were characterized by different technique: transmission electron microscopy (TEM), X-ray diffraction (XRD), laser Raman spectroscopy, scanning electron microscopy (SEM) and N_2 adsorption at −196 °C.

The effect of operating parameters such as catalyst concentrations (0.3–1.0 g L^{-1}) and initial pH (3.0–9.0) on the photocatalytic removal of atrazine was investigated. Finally, the possible atrazine degradation pathway was investigated with identification of reaction intermediates during the photocatalytic removal of atrazine using both N-TiO_2/ZSP and bare ZSP.

2. Materials and methods

2.1. Materials

Reagents used for the preparation of the photocatalysts are: titanium (IV) isopropoxide (TTIP, >97 wt%, Sigma Aldrich), ammonia aqueous solutions (30 wt%) and blue phosphors (provided by DB-Chemic, model RL-UV-B-Y, excitation wavelength: 365 nm, emission wavelength: 440 nm). The crystal structure of blue phosphors is zinc sulfide (ZnS), which emits visible light when activated with UV light [25,27].

For the photocatalytic tests, atrazine (Pestanal® by Fluka) was used.

2.2. Preparation of N-doped TiO_2 supported on phosphors

TTIP and ammonia were used as N-TiO_2 precursors.

N-TiO_2/ZSP samples were prepared by sol–gel method starting from 5 g of ZSP dispersed in a volume of TTIP ranging from 3 to 17 mL and with the addition of a volume of ammonia aqueous solution at 30 wt% in a way to have a molar ratio N/Ti equal to 18.6 [20]. The addition of ammonia aqueous solution was carried out at 0 °C, and the temperature was kept at 0 °C, while the solution was stirred vigorously, leading to the formation of a white precipitate. The precipitate was washed with water and then centrifuged. Finally, the obtained powders were heated in air up to 450 °C and maintained at this temperature for 30 min. The nominal content of N-TiO_2 on ZSP surface was varied in the range of 15–50 wt% to determine an optimal loading of N-TiO_2. The types of photocatalysts synthesized in this study and their properties are reported in Table 1.

2.3. Catalyst characterization

The synthesized catalysts were characterized by several techniques. UV–vis reflectance spectra of the catalysts were recorded by a Perkin-Elmer spectrophotometer Lambda 35 using a RSA-PE-20 reflectance spectroscopy accessory (Labsphere Inc., North Sutton, NH). All spectra were obtained using an 8° sample positioning holder, giving total reflectance relative to a calibrated standard SRS-010-99 (Labsphere Inc., North Sutton, NH). The optical band gap of each catalyst sample was determined by plotting $[F(R_\infty)^* h\nu]^2$ ($F(R_\infty)$) vs $h\nu$ (eV) and calculating the x intercept of a line passing through $0.5 < F(R_\infty) < 0.8$. As reported in literature, the determination of the band gap from the measurement of the diffuse reflectance of a powder sample is a standard technique [35]. The disk of powder sample has to be sufficiently thick that all the light that reaches the powder sample is absorbed or scattered before reaching the back surface of the sample; typically a thickness of 1–3 mm is required.

The Brunauer, Emmett and Teller (BET) surface area of the samples was measured from dynamic N_2 adsorption measurement at −196 °C, performed by a Costech Sorptometer 1042 after pretreatment at 150 °C for 30 min in He flow. XRD measurements were carried out using an X-ray micro diffractometer Rigaku D-max-RAPID, using Cu Kα radiation. Raman spectra were obtained at room temperature with a Dispersive MicroRaman (Invia, Renishaw) equipped with 514 nm diode-laser in the range of 100–2500 cm^{-1} Raman shift. The morphology and particle size were examined using a scanning electron microscope (SEM; Philips XL 30 ESEM-FEG). In addition, energy-dispersive X-ray spectroscopy (EDX) installed in ESEM was employed to observe the Ti, Zn and S distribution on the catalysts surface. A JEM-2010F (JEOL) transmission electron microscope (TEM) with a field emission gun at 200 kV was used to obtain information on the particle size and the particle structure.

The size of N-TiO_2/ZSP agglomerates was estimated by direct observation of the SEM images obtained at 800× magnification. Manual technique of evaluation of size distribution of the agglomerates involves the use of a square grid (40 × 40 mm in size) with inscribed circles of different diameters that are used to evaluate the size of the agglomerates.

Table 1
Crystallite size, SSA (BET) and optical band-gap energy of ZSP, N-TiO_2, 15N-TiO_2/ZSP 30N-TiO_2/ZSP and 50N-TiO_2/ZSP photocatalysts.

Catalyst	Nominal TiO_2 amount (wt%)	TiO_2 average crystallites size (1 0 1) (nm)	S.S.A (m^2/g)	Optical band-gap energy (eV)
ZSP	0	-	0.1	3.1
N-TiO_2	100	17	30	2.5
15 N-TiO_2/ZSP	15	9	15	3.0
30 N-TiO_2/ZSP	30	11	22	2.9
50 N-TiO_2/ZSP	50	13	29	2.6

The determination of the agglomerate average size of the different samples was accomplished by counting agglomerates and using the following equation [28]:

$$\bar{d}(\mu m) = \sum d_i \cdot f_i$$

where d_i is the size of counted agglomerates and f_i is the agglomerates size distribution estimated by

$$f_i = \frac{n_i}{\sum n_i}$$

where n_i is the number of agglomerates of size d_i.

2.4. Evaluation of photocatalytic activity

The stock solution of atrazine was prepared by dissolving the pesticide in an appropriate amount of MilliQ-grade water. A Pyrex glass (I.D. = 5 cm) Petri dish was used as the reactor. The glass reactor was sealed with Parafilm and cooled with a fan to prevent evaporation and maintain a constant temperature ($T = 27 \pm 1\,^{\circ}C$). The loading of each photocatalyst in the reaction solution was 0.5 g L^{-1} and the initial concentration of atrazine was 2.5 mg L^{-1}.

The total volume of the solution in the reactor was 15 mL. UVA-365 nm radiation was simulated by two 15 W lamps fixed at 38 mm (light intensity: 2.47 ± 0.16 mW cm^{-2}) from the upper water level in the reactor. The reactor was left in dark condition for adsorption test and under UVA illumination for removal test. Throughout the experiments, samples were taken at various time intervals. All the withdrawn samples had a volume of 100 μL and filtered with 0.45 μm pore size filters to remove the catalysts powders.

2.5. Analytical method

2.5.1. High-performance liquid chromatography (HPLC)

All analyses were performed using an Agilent 1100 Series liquid chromatography. The evaluation was carried out using a C8 column (150 mm × 4.6 mm i.d., 5 μm, Agilent), and a mobile phase consisting of 40% HPLC grade water and 60% HPLC grade acetonitrile (Tedia) (acetonitrile/H_2O = 60:40, v/v) with a flow rate of 0.4 mL min^{-1} and detection wavelength λ = 223 nm. The injected sample volume was 20 μl and the column temperature was maintained at 20 °C.

2.5.2. Intermediates identification

Intermediates identification was carried out using a combination of liquid chromatography/quadrupole time-of-flight (LC/Q-TOF) to obtain molecular weight and formula information and LC/mass spectrometry/mass spectrometry (LC/MS/MS) to determine further structural information. LC/Q-TOF analysis has been performed with an Agilent G6540A quadrupole time-of-flight mass spectrometer. Nitrogen was used as the auxiliary gas with a temperature of 300 °C and nitrogen flow rate was 7 L min^{-1}. The temperature of the sheath gas was 250 °C with a flow rate of 8 L min^{-1}.

LC/MS/MS data were acquired using the same instrument in MS/MS mode. For MS/MS modes, the same method of LC/Q-TOF analysis was used. The mobile phase consisted of 95% solvent A and 5% solvent B. Solvent A was 0.1% formic acid in water and Solvent B was 0.1% formic acid in acetonitrile. The flow rate was 0.2 mL min^{-1} and the method runtime was 5 min. An Agilent Eclipse XDB-C18 column (2.1 mm × 50 mm, 3.5 μm) was used.

3. Results and discussion

3.1. Characterization of the samples

3.1.1. Light absorption

UV–vis reflectance spectra of the photocatalysts (Fig. 1a) showed that the absorption onset shifted from about 410 nm (for ZSP alone) to 480 nm (for unsupported N-TiO_2).

The data obtained from UV–vis reflectance spectra were used for evaluating the optical band-gap energy of ZSP and N-TiO_2/ZSP by plotting $[F(R_\infty) \times h\nu]^2$ vs $h\nu$ (Fig. 1b). As shown in Fig. 1b, the increase in N-TiO_2 loading resulted in a decrease in optical band gap from 3.1 (band gap of ZPS) to 2.6 eV. Unsupported N-TiO_2 was characterized in our previous works [17,18,20]. In particular, the optical band gap was 2.5 eV. This value of optical band gap is in agreement with other studies [36,37].

The change in optical band gap is therefore attributed to the presence of N-TiO_2 on the ZSP surface, confirming the ability of photocatalysts to absorb visible light. These results are reported in Table 1. It is interesting to note that the comparison of optical band-gap evaluation for similar materials have to be performed in the same range of $h\nu$. However, when two semiconductors with specific optical band gaps are present, the evaluation could be performed in different $h\nu$ ranges. In particular, for the 30N-TiO_2/ZSP, the optical band-gap value in the common range ($0.5 < F(R_\infty) < 0.8$) is equal to 2.9 eV, very near to the optical band gap of ZnS. While, changing the range ($0.015 < F(R_\infty) < 0.026$), the obtained values are close to the optical band-gap value of N-TiO_2. These results show an additive effect of the two specific band edges on the core-shell catalyst. In the case of 15N-TiO_2/ZSP and 50N-TiO_2/ZSP catalysts, this effect could not be observed, due to the prevalence of the absorption of the phosphors support in the case of 15N-TiO_2/ZSP, and due to the prevalence of N-TiO_2 absorption in the case of 50N-TiO_2/ZSP.

3.1.2. XRD measurements

The crystal phases of N-TiO_2/ZSP catalysts were determined by XRD analysis (Fig. 2). From the XRD spectra and the corresponding characteristic 2θ values of N-TiO_2/ZSP samples (Fig. 2a) and by comparing them with the spectra of bare ZnS-based phosphors and unsupported N-TiO_2 powder (Fig. 2b), an anatase-TiO_2 peak is observed at about 25.5° for all N-TiO_2/ZSP catalysts. Moreover, ZnS-based phosphors have not undergone changes of its initial cubic face centered crystallographic structure after deposition of N-TiO_2 [25]. It is also possible to observe that with the increase in N-TiO_2 loading from 15 to 50 wt%, the intensity of the diffraction peak corresponding to anatase phase also increased.

The average size of N-TiO_2 crystallites in the pure powder and when supported on ZSP was calculated using the Scherrer equation on diffraction plane (1 0 1). The obtained results are reported in Table 1. The N-TiO_2 average crystallite size was 17 nm, according to previously characterized values [20]. On N-TiO_2/ZnS, the

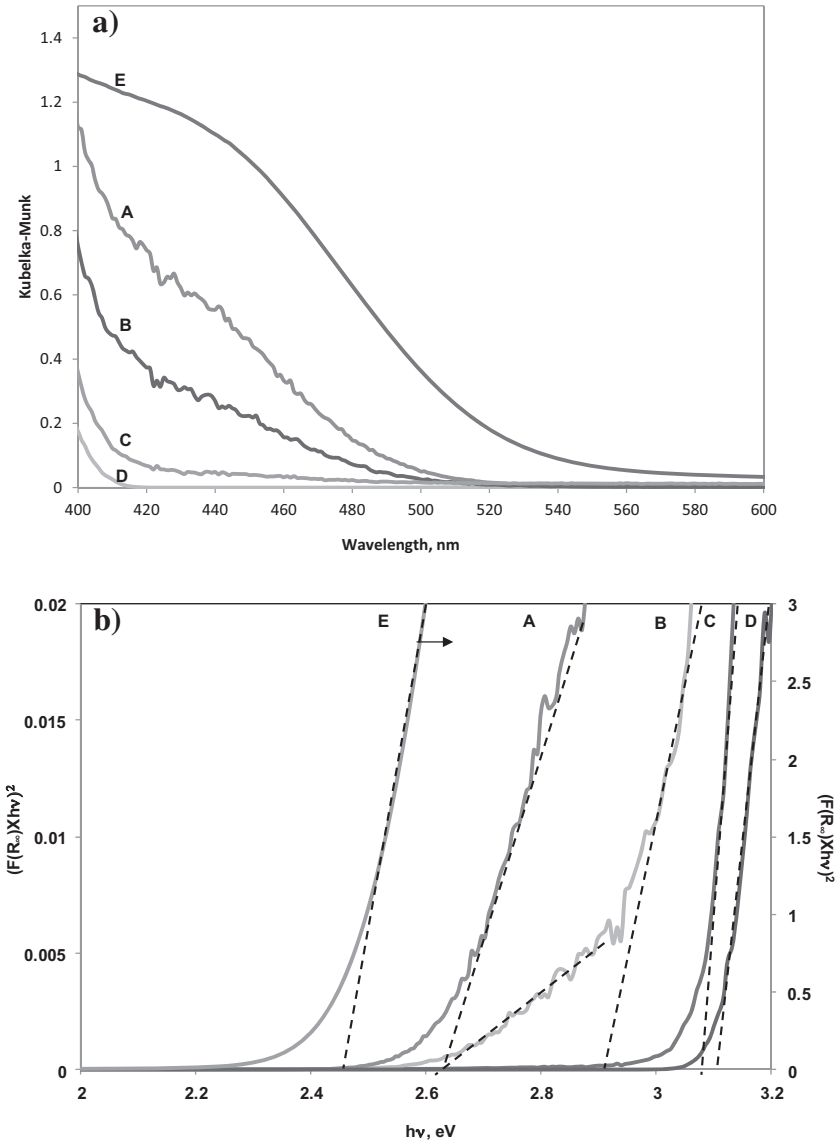

Fig. 1. UV–VIS DRS spectra (a) and band gap calculation (b) for: (A) 50N-TiO_2/ZSP, (B) 30N-TiO_2/ZSP, (C) 15N-TiO_2/ZSP, (D) ZSP, and (E) N-TiO_2 photocatalyst.

crystallite size was found smaller, with the primary particle size ranging between 9 and 13 nm. In particular, the size of the primary nanocrystallites increased with the increase in N-TiO_2 loading on ZSP surface. The size of crystallites of N-TiO_2 in the N-TiO_2/ZnS composite prepared with the sol–gel method is in agreement with the experimental results reported in the literature where for similar ZnS–TiO_2 composite the average crystallite size of TiO_2 in the ZnS–TiO_2 composite was lower than that of bare TiO_2 [42]. These results could underline the influence of support on the crystalline arrangement of N-TiO_2.

3.1.3. BET surface area measurements

The specific surface areas (SSAs) of all the samples analyzed by BET method are reported in Table 1. The SSAs of N-TiO_2 catalyst and bare ZSP sample were very different, being 30 and 0.1 $m^2\ g^{-1}$, respectively. It is interesting to note that the SSA of N-TiO_2/ZSP samples increased by increasing the N-TiO_2 loading on the surface of ZSP. Thus, since ZSP has a specific surface area of about 0.1 $m^2\ g^{-1}$, the increase in SSA is attributed to the progressive increase in N-TiO_2 amount on ZSP surface. Since the pure N-TiO_2 powder has a specific surface area of 30 $m^2\ g^{-1}$ and a crystallite size of 17 nm, and only the 50% of the composite sample is N-TiO_2, the specific surface area should be attributed to the preparation method that leads to smaller size N-TiO_2 primary nanoparticles, as shown in Table 1.

3.1.4. Raman spectra

Raman spectroscopy is an effective method to study the structure of N-TiO_2/ZSP materials because it is extremely sensitive to the crystalline phases of TiO_2 owing to its strong scattering properties [38,39]. Fig. 3 shows the Raman spectra of N-TiO_2/ZSP (Fig. 3a) in comparison with the spectrum of unsupported N-TiO_2 and bare ZSP (Fig. 3b). The spectrum of bare ZSP displayed a strong signal at 352 cm^{-1} and less intense bands at 182, 220, 404, 425, 456, 619, 643 and 674 cm^{-1} due to the Raman-active fundamental modes of ZnS [40].

15N-TiO_2/ZSP, 30N-TiO_2/ZSP and 50N-TiO_2/ZSP samples showed bands at 144, 396, 514, 637 (Fig. 3) and a weak shoulder at 195 cm^{-1} due to the Raman-active fundamental modes of anatase [41]. From the observation of the Raman spectra of N-TiO_2/ZSP samples, it was clear that the band of ZSP at 350 cm^{-1} decreased with the increase in titania loading, indicating a progressive coverage of phosphors surface by N-TiO_2. This latter issue can

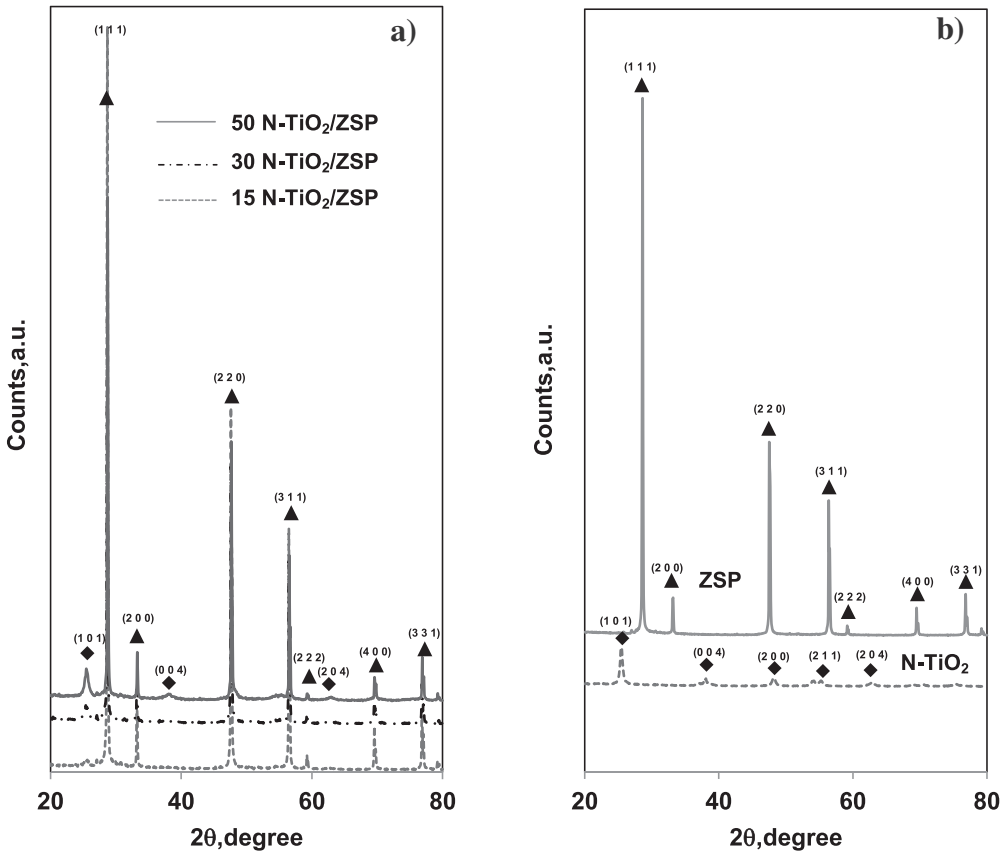

Fig. 2. (a) XRD patterns of 15 N-TiO_2/ZSP; 30 N-TiO_2/ZSP; 50 N-TiO_2/ZSP samples; (b) XRD patterns spectra of ZSP and N-TiO_2 samples. Legend: ZSP (Sphalerite cubic phase); N-TiO_2 (anatase).

be investigated using the method proposed by Quincy et al. [42]. In Fig. 4, the ratios (R) between the maximum intensity of the ZSP peaks at about 350 cm^{-1} and the maximum intensity of titania peak at 144 cm^{-1} are reported. The R value decreased with increasing the loading of N-TiO_2 in the range of 15–30 wt% on the surface of ZSP. For 50N-TiO_2/ZSP, R was about zero, indicating that almost complete coverage of ZSP surface was achieved. This result was confirmed by the value of SSA for the same sample which was about 30 $m^2\,g^{-1}$. This value was very close to that of the N-TiO_2 itself with small crystallites size, as previously underlined.

3.1.5. SEM/EDX

Fig. 5 shows the low-magnification SEM image of ZSP particles and of N-TiO_2/ZSP catalysts. The morphology of ZSP (Fig. 5a) was for most of the particles approximately spherical, or pseudo-cubical, with an average diameter of 5 μm. A smooth exposed surface of

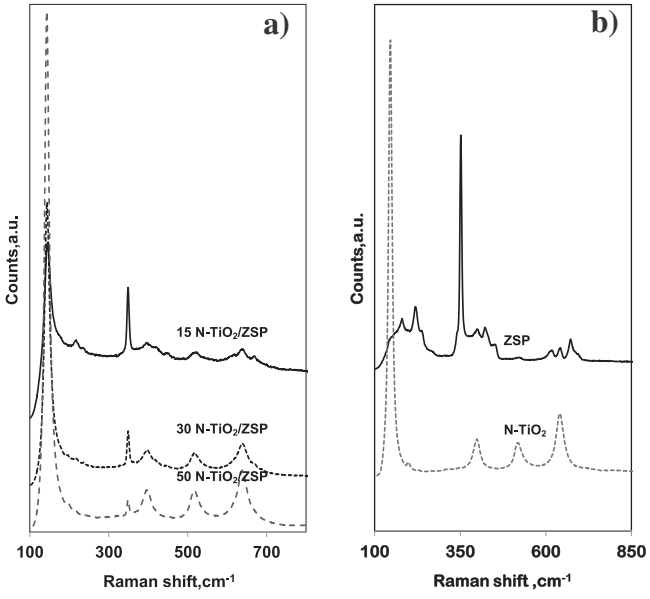

Fig. 3. (a) Raman spectra of 15 N-TiO_2/ZSP; 30 N-TiO_2/ZSP; 50 N-TiO_2/ZSP samples; (b) Raman spectra of ZSP and N-TiO_2 samples.

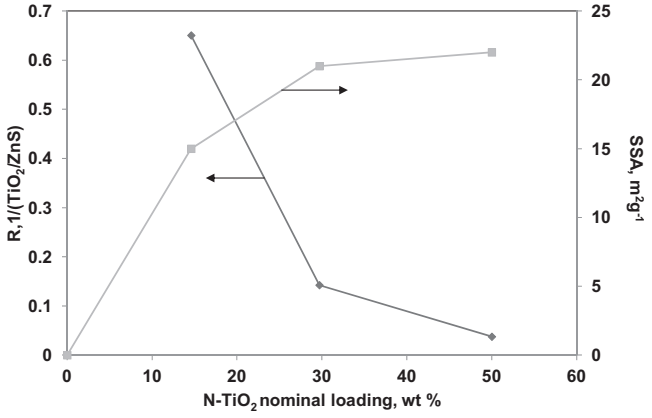

Fig. 4. Ratio between the maximum intensity of the phosphors peaks at about 350 cm^{-1} and the maximum intensity of titania peak at 144 cm^{-1} and SSA (BET) trend function of N-TiO_2 nominal loading.

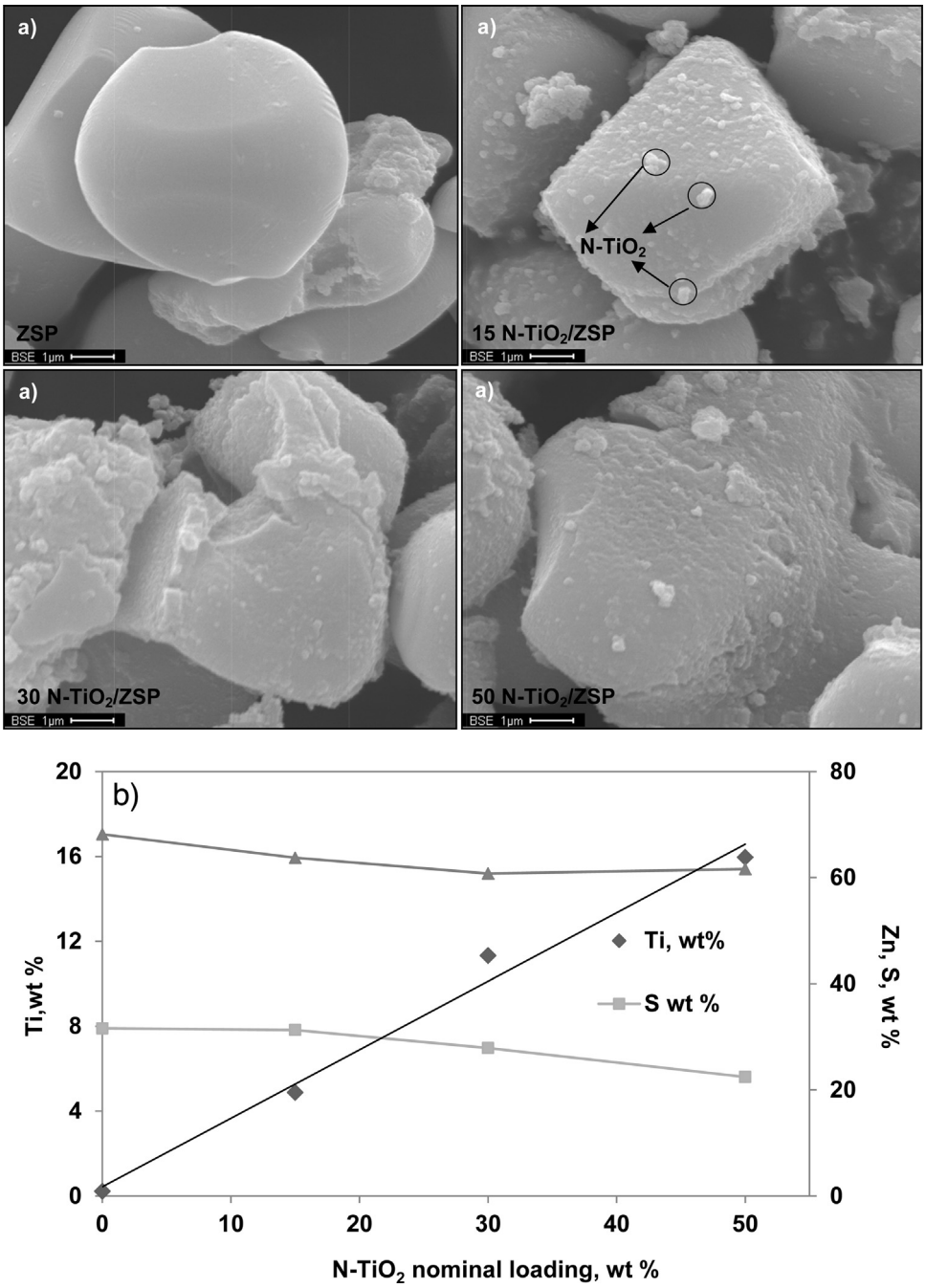

Fig. 5. (a) SEM images and (b) EDAX analysis of the samples ZSP, 15 N-TiO_2/ZSP, 30 N-TiO_2/ZSP, and 50 N-TiO_2/ZSP.

ZSP can be observed in the image. All composite samples show a similar morphology, but with an increased roughness on the surface which is attributed to the deposition of the N-TiO_2 on the surface. In Fig. 5, isles of nanoparticles of N-TiO_2 are visible in some parts. From these observations, it could be concluded that N-TiO_2 particles were rather uniformly deposited on the surface of micro-size ZSP (Fig. 5).

The atomic composition was analyzed by EDX (Fig. 5). For ZSP, it was confirmed that Zn and S were the prevalent elements with a Zn:S atomic ratio of 51:48. The molar ratio of Zn and S obtained from EDX analysis showed that S was less than Zn, but however close to the stoichiometric ratio in ZnS. In the case of N-TiO_2/ZSP samples, the amount of Zn and S decreased while the amount of Ti increased at higher loading of N-TiO_2 on the surface of ZSP as shown in Fig. 4.

3.1.6. TEM

To further characterize the nature of N-TiO_2 supported on the surface of ZSP, TEM analysis was performed. TEM images with a resolution of 5 μm are reported in Fig. 6a–d. The ZSP particles appear black due to their size (Fig. 6a). When N-TiO_2 is present on the ZSP surface, a thin layer of nanoparticles can be observed (Fig. 6b–d) and it was evidenced by a yellow color. When N-TiO_2 was deposited on the surface of ZSP, a uniform coverage with small agglomerate was formed for the sample 15N-TiO_2/ZSP (Fig. 6b). The nanoparticles seem to be well dispersed on the ZPS surface, and the thickness

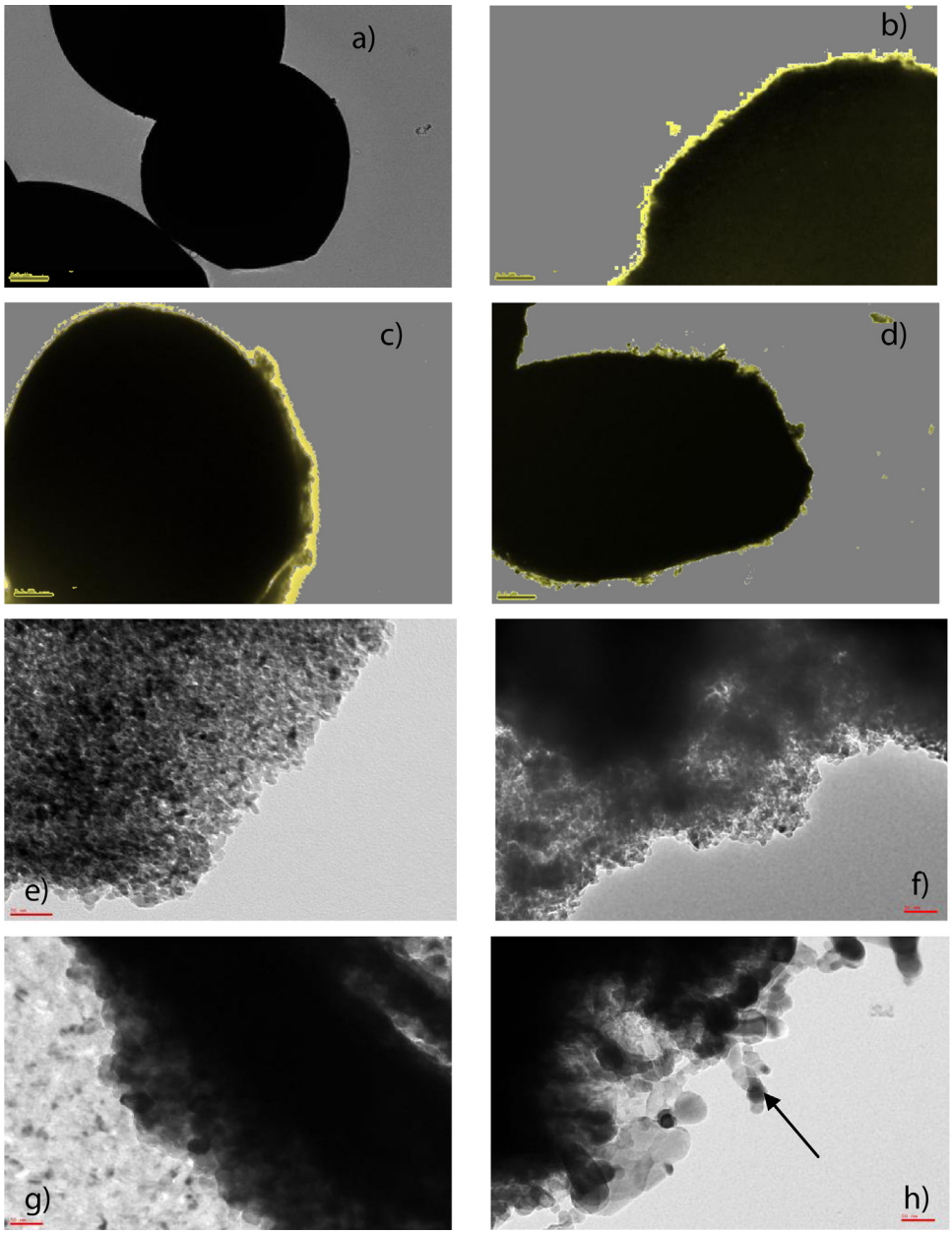

Fig. 6. TEM images: (a) ZSP; (b) 15 N-TiO_2/ZSP; (c) 30 N-TiO_2/ZSP; (d) 50 N-TiO_2/ZSP (scale bar equal to 5 μm); (e) N-TiO_2; (f) 15 N-TiO_2/ZSP; (g) 30 N-TiO_2/ZSP; (h) 50 N-TiO_2/ZSP (scale bar equal to 50 nm).

clearly increases passing from 15 to 30 wt% of N-TiO_2 supported. For 50N-TiO_2/ZPS composite, it is not easy to observe the thickness of the layer, probably due to its high compactness. However, due to the high amount of N-TiO_2, some ZPS particles appear to possess a certain adherence. Moreover, it is possible to observe the formation of N-TiO_2 nanoparticles islands for the sample 50N-TiO_2/ZSP (Fig. 6d).

Fig. 6 also shows the TEM images with a higher resolution, 50 nm (Fig. 6e–h). In this case, it is interesting to observe that the pseudo-spherical crystallites of unsupported N-TiO_2 (Fig. 6e) do not change when supported on the surface of ZSP (15N-TiO_2/ZSP, Fig. 6g). By increasing the loading of N-TiO_2 (30N-TiO_2/ZSP, Fig. 6f), a part of the layer shows an increased density of nanoparticles. Moreover, passing from 15N-TiO_2/ZSP (Fig. 6f) to 30N-TiO_2/ZSP, an increase in N-TiO_2 size was observed in the latter catalyst (Fig. 6g). For the sample 50N-TiO_2/ZSP (Fig. 6h), an increased nanoparticle density and size and also a change in N-TiO_2 crystallite shape was observed. The almost rare appearance of elongated particles could be an indication of a possible interaction between ZSP and N-TiO_2.

3.1.7. *Agglomerate size analysis*

The size of ZSP and the agglomeration of N-TiO_2/ZSP particles have been investigated using SEM images with a magnification of 800×. As shown in Fig. 7, the deposition of N-TiO_2 on the ZSP surface determined a change of particle agglomeration. For the lower amount of N-TiO_2 on ZSP, it is possible to observe small agglomerates (Fig. 7a and b), while by increasing the load of N-TiO_2, the number and the size of the agglomerates tend to increase (Fig. 7c and d). In particular, the size distribution of the agglomerates, evaluated from the direct observation of SEM images, is reported in Fig. 8. The average agglomerate size was about 5 μm for the samples ZSP, 15N-TiO_2/ZSP and 30N-TiO_2/ZSP and increased up to a value of about 10 μm for the sample 50N-TiO_2/ZSP.

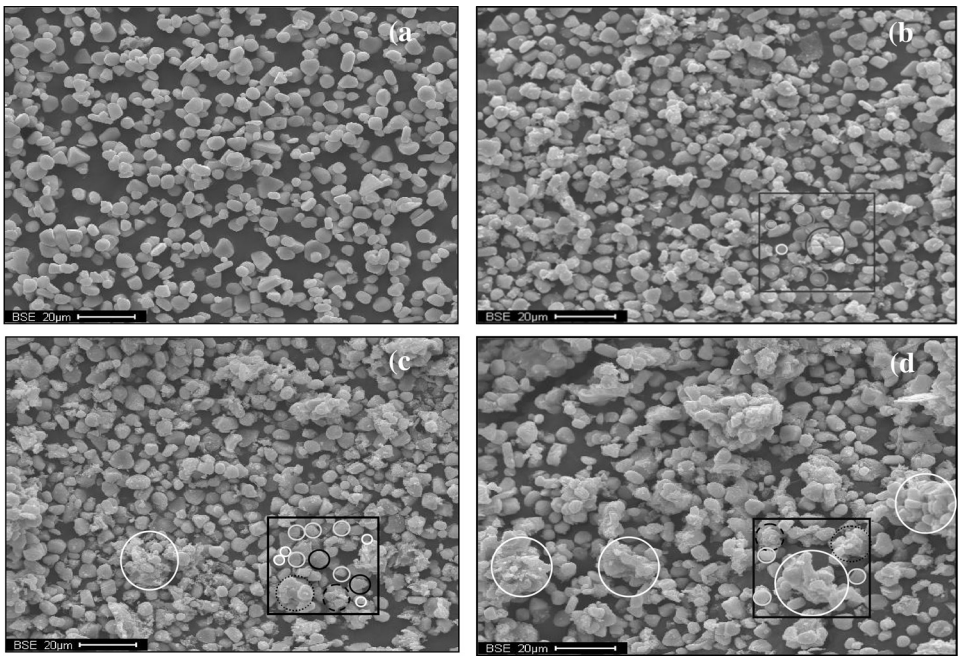

Fig. 7. SEM imagines of (a) ZSP; (b) 15 N-TiO_2/ZSP; (c) 30 N-TiO_2/ZSP; (d) 50 N-TiO_2/ZSP.

3.2. Photocatalytic activity of N-TiO_2/ZSP catalysts

3.2.1. Influence of N-TiO_2 loading

Fig. 9 shows the experimental data of the removal of atrazine at an initial pH of 5.8 and photocatalyst loading of 0.5 g L^{-1}. All catalyst samples effectively removed atrazine. The removal of atrazine was 54, 94 and 78% for 15N-TiO_2/ZSP, 30N-TiO_2/ZSP and 50N-TiO_2/ZSP, respectively, after 90 min. On the other hand, bare ZSP and N-TiO_2 only demonstrated lower atrazine removal compared to all N-TiO_2/ZSP. The removal of atrazine was 41% for bare ZSP and 45% for N-TiO_2 only. It is important to note that the photocatalytic activity of phosphors alone was very similar to that of N-TiO_2 only. This behavior has been attributed to the ability of ZnS to photogenerate surface SH group and OH radicals in the presence of water and UVA irradiation [43]. As a confirmation of the general mechanism of photocatalytic oxidation induced by the presence of water on the surface of ZnS, it must be noted that no photoactivity was observed when the same kind of phosphors are used in the gas phase photoreactions and this could be justified by the low amount of water employed for the tests [27].

30N-TiO_2/ZSP sample showed the highest photocatalytic activity under the experimental conditions. The pesticide concentration

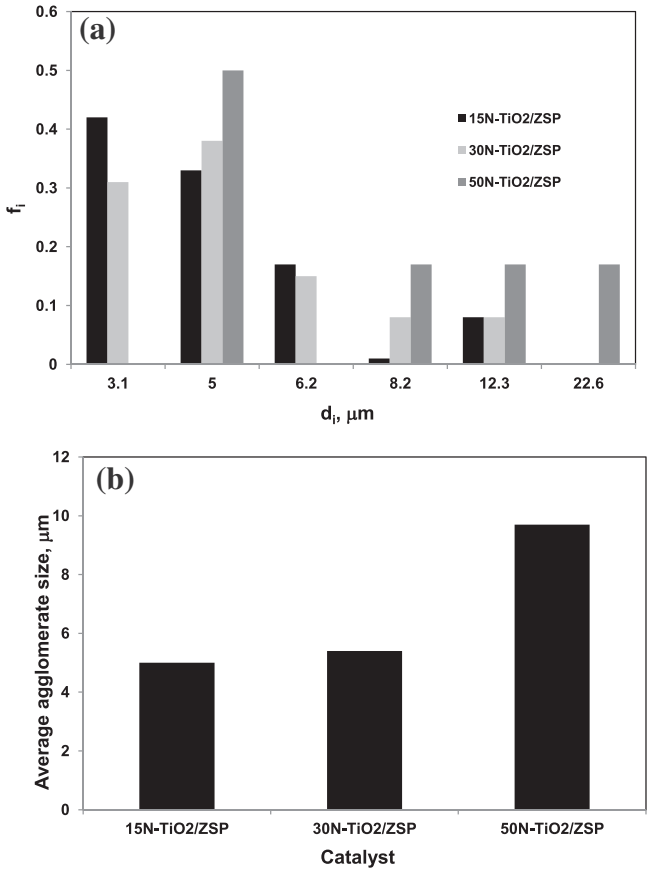

Fig. 8. Agglomerate size distribution (a) and average agglomerate size (b) estimated from SEM images.

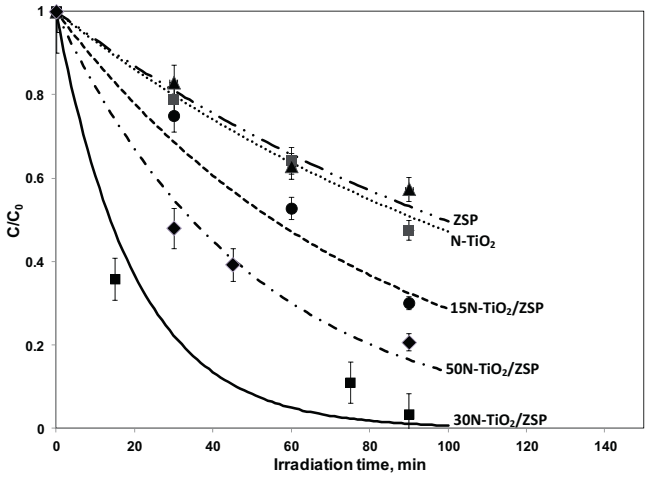

Fig. 9. Behavior of atrazine experimental concentration (symbols) and predicted data (lines) as function of irradiation time for the different photocatalysts.

decreased rapidly within the first 15 min and reached almost zero after about 90 min (Fig. 9). The photocatalytic activity of 30N-TiO_2/ZSP was significantly enhanced because the surface of ZSP was not fully covered by N-TiO_2 nanoparticles, allowing the activation of ZSP by UV for visible light emission. The emitted visible light from ZSP has activated effectively N-TiO_2 on the surface of ZSP, resulting in the highest removal of atrazine. The obtained result evidenced that by supporting N-TiO_2 photocatalyst on ZSP surface allows a dramatic enhancement in the removal of atrazine.

3.2.2. Evaluation of apparent degradation kinetic constant

The apparent kinetic constant was evaluated considering the pseudo-first-order kinetics.

Atrazine mass balance can be written as

$$\frac{dC(t)}{dt} = -kCa \quad (1)$$

where $C(t)$ is the atrazine concentration (mg L^{-1}), k the apparent kinetic constant (L g^{-1} min^{-1}) and a the N-TiO_2 effective dosage (considering the N-TiO_2 content in N-TiO_2/ZSP catalysts) (g L^{-1}).

The initial condition was

$t = 0\, C_0 = 2.5 \text{mg } L^{-1}$.

The values of a, used in Eq. (1), have been calculated as follows:

$$a = \frac{W_{\text{N-TiO}_2}}{100} \cdot d \quad (2)$$

where $W_{\text{N-TiO}_2}$ is the N-TiO_2 content in N-TiO_2/ZSP (wt%) and d the N-TiO_2/ZSP dosage = 0.5 g L^{-1}.

Eq. (1) was solved by the Euler iterative method. Primary goal of the simulation by the mathematical model is to identify the apparent kinetic constant k using nonlinear regression analysis of the experimental data reported in Fig. 9 as a function of irradiation time. The nonlinear regression procedure was performed using the least-squares approach, based on the minimization of the sum of squared residuals between the experimental data and the values given by the mathematical model. The fitting procedure has allowed to obtain the following values for k: 0.015, 0.014, 0.15, 0.25 and 0.09 L $g_{\text{N-TiO2}}{}^{-1}$ min^{-1} for ZSP, N-TiO_2, 15N-TiO_2/ZSP, 30N-TiO_2/ZSP and 50N-TiO_2/ZSP, respectively.

The estimated k is independent from the overall amount of catalyst and only correlated to the N-TiO_2 active phase loaded on the ZSP surface. It is important to note that the kinetic constant for N-TiO_2/ZSP photocatalysts is about 10 times higher than the kinetic constants of ZSP and N-TiO_2.

The obtained results are summarized in Fig. 10, which also reports the average agglomerate size of photocatalysts as function of N-TiO_2 loading. The apparent kinetic constant increased almost linearly until N-TiO_2 loading of 30 wt%. In the range of N-TiO_2 loading from 0 to 30 wt%, the average agglomerate size of each sample was similar (almost 5 μm). On the other hand, the SSA, also reported in Fig. 10, increased up to the N-TiO_2 loading of 30 wt%. Therefore, the increase in photocatalytic activity in the range 0–30 wt% is correlated only to the increase in specific surface area of the photocatalysts.

When N-TiO_2 loading was higher than 30 wt%, the photocatalytic activity decreased. In fact, the apparent kinetic constant of atrazine removal for 50N-TiO_2/ZSP (0.09 L $g_{\text{N-TiO2}}{}^{-1}$ min^{-1}) was lower than that of 30N-TiO_2/ZSP (0.25 L $g_{\text{N-TiO2}}{}^{-1}$ min^{-1}). In this case, the decrease in reaction rate could be related to the increase in N-TiO_2 agglomerate size, from about 5 μm up to 10 μm, observed by increasing N-TiO_2 loading from 30 to 50 wt%. From these results, it could be argued that the tendency to the agglomeration, and consequently the size of agglomerates, may influence the ability of the different N-TiO_2/ZSP samples to remove the atrazine. This phenomenon has been previously observed in the *Escherischia coli* inactivation on N-TiO_2 photocatalyst [17]. From these results, it is concluded that the best catalyst is 30N-TiO_2/ZSP. Therefore, this last catalyst was chosen to investigate the influence of catalyst dosage and initial pH of atrazine solution.

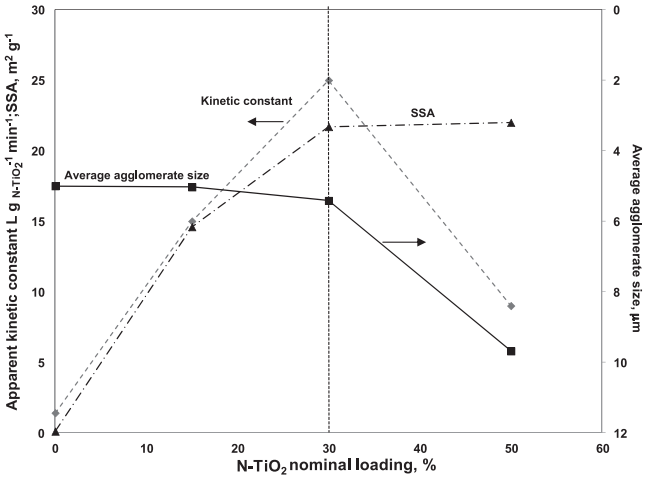

Fig. 10. Atrazine apparent kinetic constant, catalysts average agglomerate size, and specific surface areas (SSA) as a function of N-TiO_2 nominal loading.

3.2.3. Optimization of 30N-TiO_2/ZSP dosage in aqueous suspension

To study the effect of 30N-TiO_2/ZSP dosage on the removal of atrazine, the catalyst concentration was varied from 0.3 to 1.0 g L^{-1}. The initial concentration of atrazine was 2.5 mg L^{-1} for all experiments. Fig. 11 shows the effect of the catalyst dosage on atrazine removal after 60 min of irradiation.

It was observed that the removal rate increased proportionally until a photocatalyst loading of 0.5 g L^{-1}. A further increase in catalyst dosage determined a decrease in atrazine removal rate. This phenomenon may be due to the increase in agglomeration tendency [44] between 30N-TiO_2/ZSP particles in aqueous suspension, causing an increase in light scattering phenomena and the decrease in light penetration in the core of the reactor. In particular, a high amount of 30N-TiO_2/ZSP in the reactor could induce the appearance of photon limitations phenomena due to the formation of large agglomerates that decrease the ZSP surface able to capture the UVA light emitted by the light source, resulting in loss of the advantages to use ZSP as a supporting material for N-TiO_2 photocatalysts.

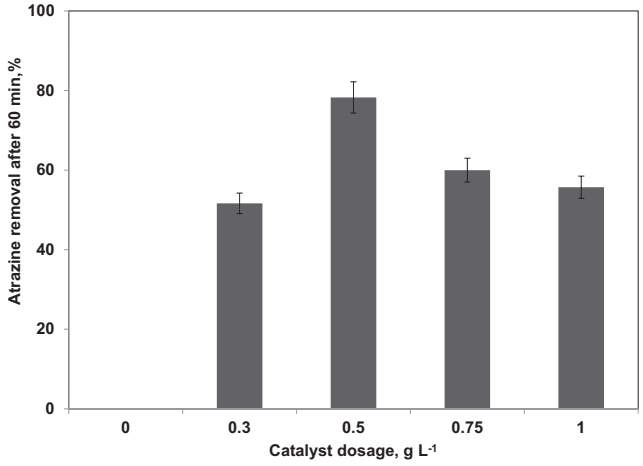

Fig. 11. Effect of 30 N-TiO_2/ZSP dosage on the removal of atrazine.

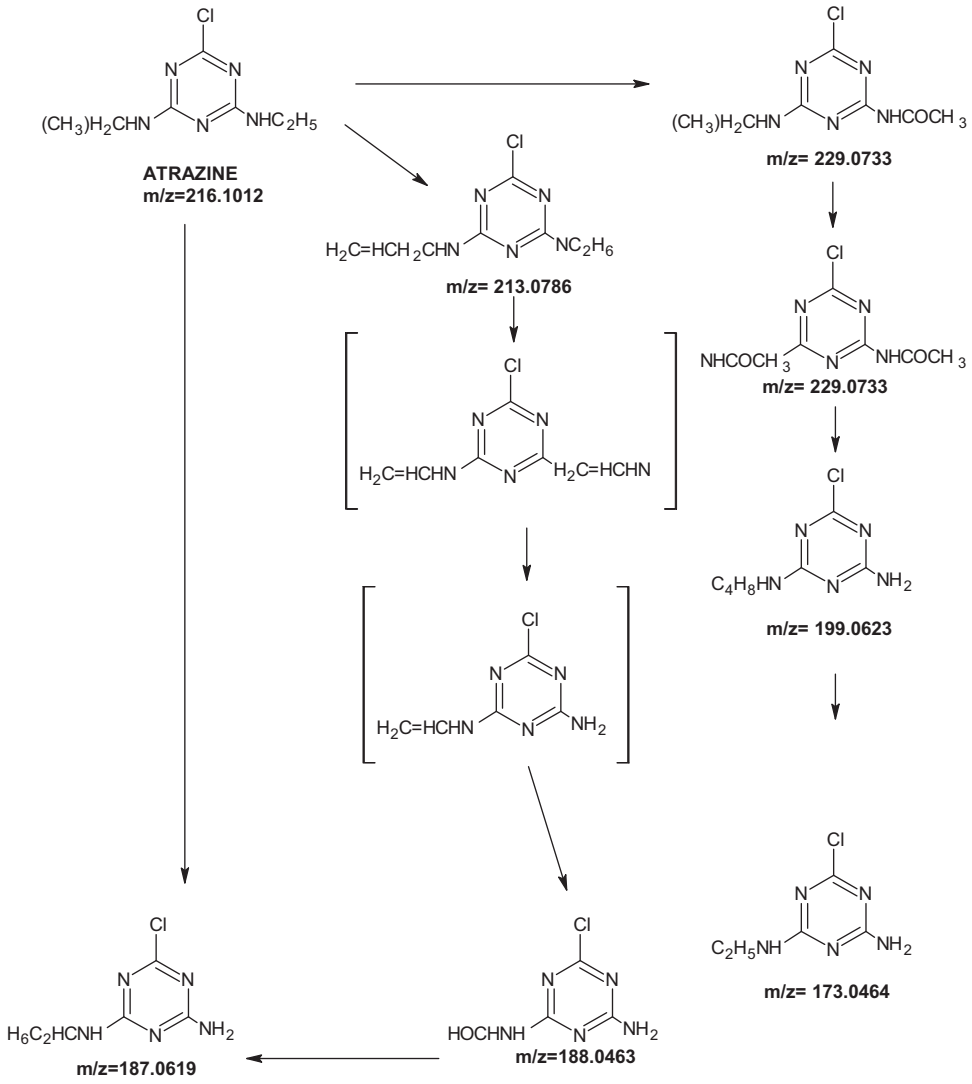

Scheme 1. Possible degradation pathway of atrazine by ZSP under UVA irradiation.

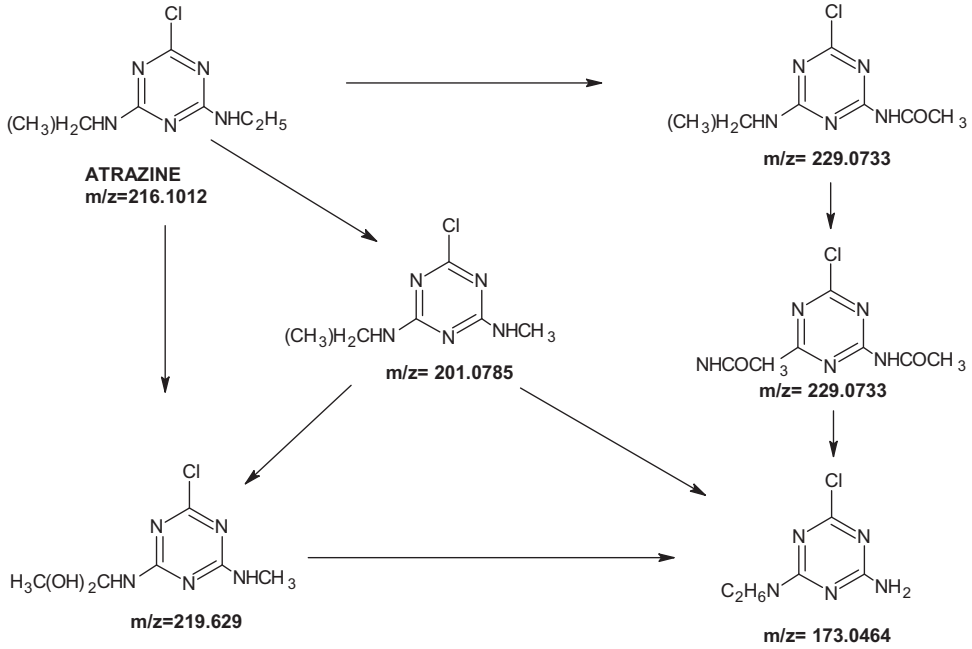

Scheme 2. Possible degradation pathway of atrazine by 30 N-TiO_2/ZSP under UVA irradiation.

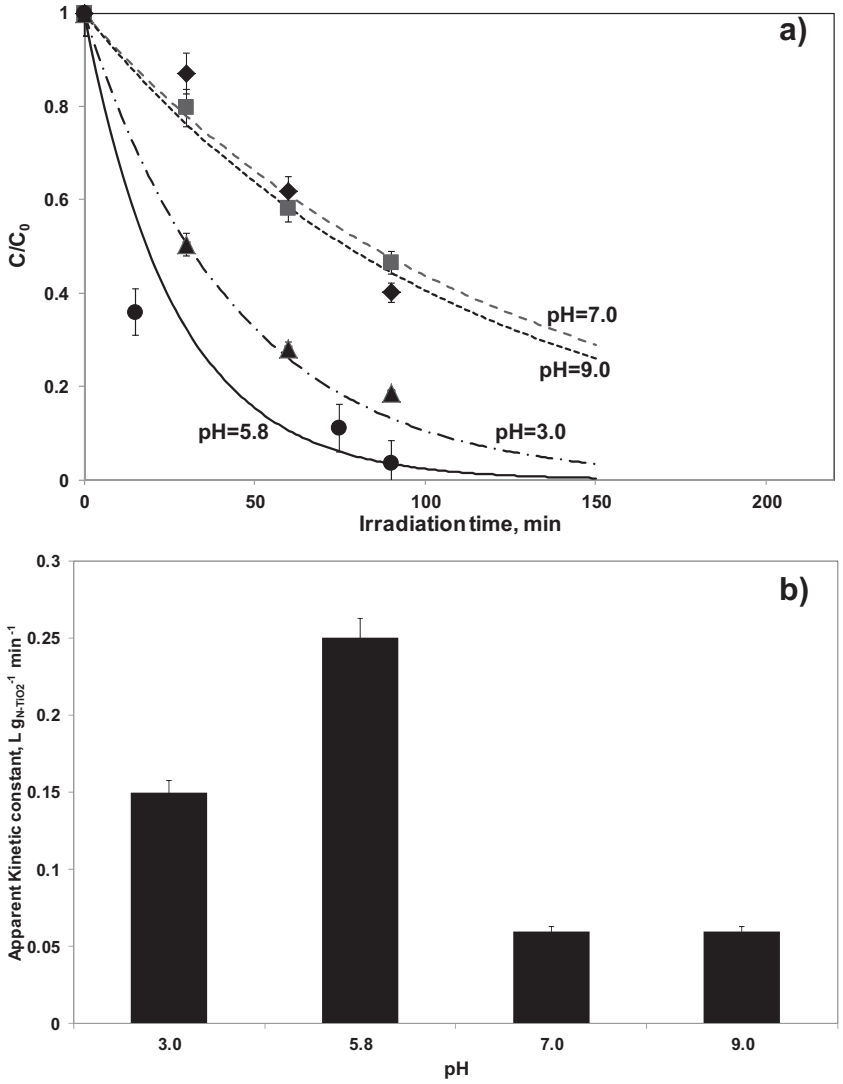

Fig. 12. (a) Behavior of atrazine experimental concentration (symbols) and predicted data (lines) as function of irradiation time for 30 N-TiO_2/ZSP at different initial pH values, and (b) apparent kinetic constant at different initial pH values.

3.2.4. Influence of pH

To study the effect of pH in the removal of atrazine, the initial pH of the solution was changed in the range from 3.0 to 9.0 and 30N-TiO_2/ZSP sample was used. The trend of atrazine removal in the presence of different initial pH (shown in Fig. 12a) showed that the best atrazine removal has been obtained at initial pH of 5.8 in which the atrazine removal reached the value of about 94% after 90 min of irradiation. In contrast, a stronger acidic condition (pH 3.0) resulted in a lower removal value, equal to 82%.

When the initial solution pH increased, in particular, at pH 7.0 and 9.0, the atrazine removal decreased to 60 and 53%, respectively. The obtained experimental data were used for the evaluation of apparent kinetic constant that, as shown in Fig. 12b, increased from 0.15 to 0.25 L $g_{N\text{-}TiO2}{}^{-1}$ min^{-1} for pH 3.0 and 5.8, respectively, and then decreased to 0.06 L $g_{N\text{-}TiO2}{}^{-1}$ min^{-1} for pH 7.0 and 9.0. The obtained trend is in agreement with experimental data reported in the literature concerning the photocatalytic removal of atrazine [45].

In particular, at pH 7.0, and at higher pH values, equal to 9.0, the change in surface charge of photocatalysts leads to surface electrostatic repulsion phenomena leading to a lower removal rate [45].

3.2.5. Reaction Intermediates

Reaction intermediates were observed during the photocatalytic decomposition of atrazine using 30N-TiO_2/ZSP and ZSP.

Before analyzing the reaction intermediates on 30N-TiO_2/ZSP, the intermediates formed in the presence of bare ZSP were analyzed. The following molecular fragments m/z were identified: 229.0733, 213.0786, 199.0623, 188.0463, 187.0619 and 173.0464. Some of the molecular fragments identified (m/z = 229.0733 and 173.0464) are the same as those found in the presence of TiO_2 [46,47]. The chemical formulas for intermediates were provided by the mass accuracy of the instrument and these formulas were compared with the literature data to identify molecular structures [48–50].

Based on the structures of the intermediates detected during the degradation, the main pathway of atrazine photocatalytic degradation for ZSP was proposed in the Scheme 1. The reaction mainly involved dealkylation reactions and alkyl chain oxidation. It is important to underline that no dechlorination of aromatic structure occurred after 30 min of irradiation, meaning that cyanuric acid (1,3,5-triazine-2,4,6-triol, $C_3N_3(OH)_3$), previously reported in literature for photocatalytic degradation of atrazine using TiO_2 as photocatalysts [46,47], was not formed. Cyanuric acid was not detected also after long irradiation time (24 h). The absence of this

contaminant, which resists to the oxidation by hydroxyl radicals [45], is a very important issue.

In comparison with bare ZSP, different intermediates with m/z = 201.0785 and 219.629 were observed during the photocatalysis using N-TiO_2/ZSP. Also, in this case, the mass accuracy of the instrument is sufficient to provide chemical formulas for these intermediates and the structure was incorporated in Scheme 2. Intermediates with similar chemical structure were previously reported in the literature on PF-codoped TiO_2 [51]. Also, with 30N-TiO_2/ZSP, dechlorination of atrazine was not observed and the main reactions were dealkylation and alkyl chain oxidation [51]. Comparing Schemes 1 and 2, the first information was that the intermediates with m/z = 229.0733 and 173.0464 were likely formed on the ZSP surface not covered by N-TiO_2 particles. However, the presence of N-TiO_2 particles dispersed on ZSP surface leading to a change of selectivity because on 30N-TiO_2/ZSP, two different compounds with m/z = 201.0785 and 219.629 appeared (Scheme 2) inhibiting the formation of intermediates with m/z = 213.0786, 199.0623, 188.0463 and 187.0619 (Scheme 1). The experimental data evidenced that, probably, the presence of ZSP did not induce the dechlorination of atrazine that leads to the formation of cyanuric acid, which is the typical final product of photocatalytic degradation of atrazine in presence of TiO_2-based photocatalysts [45].

4. Conclusions

Visible light-active N-TiO_2 photocatalyst was successfully deposited on ZnS-based luminescent phosphors microparticles (ZSP) by a modified sol–gel method. Compared to the single materials, the synthesized composite photocatalysts (N-TiO_2/ZSP) exhibited enhancement in photocatalytic activity for the removal of atrazine. With the increase in N-TiO_2 loading, the size of primary nanoparticles on the ZSP support increased, however being always smaller than that of pure N-TiO_2. From the TEM images, it was observed, respectively, an increase in the thickness of N-TiO_2 layer with an increase in the N-TiO_2 loading. This resulted in a higher specific surface area, mainly due to N-TiO_2 exposed.

The results showed that N-TiO_2/ZSP photocatalysts are very efficient to remove atrazine under UVA illumination. The photocatalyst N-TiO_2/ZPS with N-TiO_2 loading of 30 wt% was the most active. In particular, 94% of atrazine was degraded after 90 min of UVA irradiation compared to N-TiO_2 only (45%). The apparent kinetic constant estimated for all the photocatalysts with a pseudo-first-order kinetic model was one order of magnitude or more higher than those of the single components, showing a “synergistic” photocatalytic effect. The apparent kinetic constant increased with the specific surface area up to 30 wt% of N-TiO_2 loading. Beyond the optimal loading of N-TiO_2 (30 wt%), the photocatalytic activity decreased because of the increase in N-TiO_2 agglomerate size. The photocatalytic atrazine conversion strongly depended on catalyst loading and the initial pH of solution. The higher extent of degradation was found at 0.5 g L^{-1} and at pH of 5.8. A possible degradation pathway was proposed by the identification of the reaction intermediates during the photocatalysis using 30N-TiO_2/ZSP and ZSP. The degradation mainly involved dealkylation reaction and alkyl chain oxidation both in the presence of 30N-TiO_2/ZSP and ZSP. However, the presence of N-TiO_2 particles dispersed on ZSP surface led to a change in selectivity, lowering the number of intermediates formed during irradiation. It is important to underline that, in the presence of ZSP support, no dechlorination of aromatic structure occurred, and thus no formation of cyanuric acid was observed.

This study clearly demonstrates the importance of using the ZSP as a supporting material for N-TiO_2 nanoparticles. ZSP phosphors increased the removal rate of atrazine, due to both visible light emitted by them and to the intrinsic photoactivity of ZnS because of its semiconducting properties.

Acknowledgements

This work was partially funded by the Cyprus Research Promotion Foundation through Desmi 2009-2010 which is co-funded by the Republic of Cyprus and the European Regional Development Fund of the EU under contract number NEA IPODOMI/STRATH/0308/09. C.H. is the recipient of the Graduate School Dean’s Fellowship, which supports the University of Cincinnati doctoral students in their final year of degree work. D.S. wishes to thank the University of Salerno for funding the project “Processi catalitici innovativi per la depurazione ambientale” (Ex 60%, anno 2012).

References

[1] J. Anon, Am. Water Works Assoc. 87 (1995) 122.
[2] F. Gianturco, C.M. Chiodaroli, I.R. Bellobono, M.L. Raimondi, A. Moroni, B. Gawlik, Fresenius Environ. Bull. 6 (1997) 461–468.
[3] E. Pelizzetti, V. Maurino, C. Minero, V. Carlin, E. Pramauro, O. Zerbinati, M.L. Tosato, Environ. Sci. Technol. 24 (1990) 1559–1565.
[4] E. Pelizzetti, V. Carlin, V. Maurino, C. Minero, M. Dolci, A. Marchesini, Soil Sci. 150 (1990) 523–526.
[5] I. Texier, J. Ouazzani, J. Delaire, C. Giannotti, Tetrahedron 55 (1999) 3401–3412.
[6] I.K. Konstantinou, T.M. Sakellarides, V.A. Sakkas, T.A. Albanis, Environ. Sci. Technol. 35 (2001) 398–405.
[7] M. Lackhoff, R. Niessner, Environ. Sci. Technol. 36 (2002) 5342–5347.
[8] H. Labiadh, T. Ben Chaabane, L. Balan, N. Becheik, S. Corbel, G. Medjahdi, R. Schneider, Appl. Catal. B 144 (2014) 29–35.
[9] Y.J. Kim, B. Gao, S.Y. Han, M.H. Jung, A.K. Chakraborty, T. Ko, C. Lee, W.I. Lee, J. Phys. Chem. C 113 (2009) 19179–19184.
[10] Y. Huang, F. Sun, T. Wu, Q. Wu, Z. Huang, H. Su, Z. Zhang, J. Solid State Chem. 184 (2011) 644–648.
[11] C. Harris, P.V. Kamat, ACS Nano 3 (2009) 682–690.
[12] B. Ma, L. Wang, H. Dong, R. Gao, Y. Geng, Y. Zhu, Y. Qiu, Phys. Chem. Chem. Phys. 13 (2011) 2656–2658.
[13] K.P. Acharya, T.R. Alabi, N. Schmall, N.N. Hewa-Kasakarage, M. Kirsanova, A. Nemchinov, E. Khon, M. Zamkov, J. Phys. Chem. C 113 (2009) 19531–19535.
[14] C. Petrier, B. David, S. Laguian, Chemosphere 32 (1996) 1709–1718.
[15] V. Vaiano, O. Sacco, D. Sannino, P. Ciambelli, S. Longo, V. Venditto, G. Guerra, J. Chem. Technol. Biotechnol. 89 (2014) 1175–1181.
[16] V. Vaiano, O. Sacco, D. Sannino, P. Ciambelli, Chem. Eng. J. (2014), http://dx.doi.org/10.1016/j.cej.2014.02.071
[17] L. Rizzo, D. Sannino, V. Vaiano, O. Sacco, A. Scarpa, D. Pietrogiacomi, Appl. Catal. B: Environ. 144 (2014) 369–378.
[18] D. Sannino, V. Vaiano, O. Sacco, P. Ciambelli, J. Environ. Chem. Eng. 1 (2013) 56–60.
[19] M. Antoniadou, V. Vaiano, D. Sannino, P. Lianos, Chem. Eng. J. 224 (2013) 144–148.
[20] O. Sacco, M. Stoller, V. Vaiano, P. Ciambelli, A. Chianese, D. Sannino, Int. J. Photoenergy 2012 (2012), Article ID 626759, 8 pages, http://dx.doi.org/10.1155/2012/626759
[21] C. Han, M. Pelaez, V. Likodimos, A.G. Kontos, P. Falaras, K. O'Shea, D.D. Dionysiou, Appl. Catal. B 107 (2011) 77–87.
[22] S. Sato, Chem. Phys. Lett. 123 (1986) 126–128.
[23] V. Palma, D. Sannino, V. Vaiano, P. Ciambelli, Ind. Eng. Chem. Res. 49 (2010) 10279–10286.
[24] V. Vaiano, O. Sacco, M. Stoller, A. Chianese, P. Ciambelli, D. Sannino, Int. J. Chem. Reactor Eng. 12 (2014).
[25] D. Sannino, V. Vaiano, P. Ciambelli, Catal. Today 205 (2013) 159–167.
[26] D. Sannino, V. Vaiano, P. Ciambelli, G. Carotenuto, M. Di Serio, E. Santacesaria, Catal. Today 209 (2013) 159–163.
[27] P. Ciambelli, D. Sannino, V. Palma, V. Vaiano, R.S. Mazzei, Photochem. Photobiol. Sci. 10 (2011) 414–418.
[28] J.J. Murcia, M.C. Hidalgo, J.A. Navío, V. Vaiano, P. Ciambelli, D. Sannino, Int. J. Photoenergy 2012 (2012), Article ID 687262, 9 pages, http://dx.doi.org/10.1155/2012/687262
[29] A. Guillén-Santiago, S.A. Mayén, G. Torres-Delgado, R. Castanedo-Pérez, A. Maldonado, M.D.L.L. Olvera, Mater. Sci. Eng. B: Solid-State Mater. Adv. Technol. 174 (2010) 84–87.
[30] N. Murakami, T. Chiyoya, T. Tsubota, T. Ohno, Appl. Catal. A: Gen. 348 (2008) 148–152.
[31] E.M. Rockafellow, L.K. Stewart, W.S. Jenks, Appl. Catal. B: Environ. 91 (2009) 554–562.
[32] H. Ozaki, N. Fujimoto, S. Iwamoto, M. Inoue, Appl. Catal. B: Environ. 70 (2007) 431–436.
[33] C. Di Valentin, G. Pacchioni, Catal. Today 206 (2013) 12–18.

[34] S. Livraghi, M.C. Paganini, E. Giamello, A. Selloni, C. Di Valentin, G. Pacchioni, J. Am. Chem. Soc. 128 (2006) 15666–15671.
[35] B. Karvaly, I. Hevesi, Z. Naturforsch. A 26 (1971) 245–249.
[36] W. Guo, Y. Shen, G. Boschloo, A. Hagfeldt, T. Ma, Electrochim. Acta 56 (2011) 4611–4617.
[37] L.M.A. Franco, G. Zambrano, M.E. Gomez, E. Camps, L. Escobar-Alarcon, Superficies Vacio 25 (2012) 161–165.
[38] X. Gao, S.R. Bare, J.L.G. Fierro, M.A. Banares, I.E. Wachs, J. Phys. Chem. B 102 (1998) 5653–5666.
[39] X. Yu, Q. Wu, S. Jiang, Y. Guo, Mater. Charact. 57 (2006) 333–341.
[40] W.G. Nilsen, Second-order Raman Spectra of Some Zinc Blende and Wurtzite Crystals, Springer, New York, 1969, pp. 129–137.
[41] L.J. Alemany, L. Lietti, N. Ferlazzo, P. Forzatti, G. Busca, E. Giamello, F. Bregani, J. Catal. 155 (1995) 117–130.
[42] R.B. Quincy, M. Houalla, D.M. Hercules, J. Catal. 106 (1987) 85–92.
[43] J. Kim, M. Kang, Bull. Kor. Chem. Soc. 33 (2012) 2133–2139.
[44] J. Cunningham, P. Sedlak, Catal. Today 29 (1996) 309–315.
[45] S. Parra, S.E. Stanca, I. Guasaquillo, K. Ravindranathan Thampi, Appl. Catal. B: Environ. 51 (2004) 107–116.
[46] C. Qin, S. Yang, C. Sun, M. Zhan, R. Wang, H. Cai, J. Zhou, Frontiers Environ. Sci. Eng. China 4 (2010) 321–328.
[47] T.A. McMurray, P.S.M. Dunlop, J.A. Byrne, J. Photochem. Photobiol. A: Chem. 182 (2006) 43–51.
[48] C. Chen, S. Yang, Y. Guo, C. Sun, C. Gu, B. Xu, J. Hazard. Mater. 172 (2009) 675–684.
[49] K.H. Chan, W. Chu, J. Agric. Food Chem. 54 (2006) 1804–1813.
[50] J. Andersen, M. Pelaez, L. Guay, Z. Zhang, K. O'Shea, D.D. Dionysiou, J. Hazard. Mater. 260 (2013) 569–575.
[51] J.A. Khan, C. Han, N.S. Shah, H.M. Khan, M.N. Nadagouda, V. Likodimos, P. Falaras, K. O'Shea, D.D. Dionysiou, Environ. Eng. Sci. 31 (2014) 435–445.